PHYSICAL REVIEW B **98**, 201105(R) (2018)

Rapid Communications

Covalency-driven collapse of strong spin-orbit coupling in face-sharing iridium octahedra

Mai Ye,[1,*] Heung-Sik Kim,[1,†] Jae-Wook Kim,[1] Choong-Jae Won,[2,3] Kristjan Haule,[1] David Vanderbilt,[1]
Sang-Wook Cheong,[1,4] and G. Blumberg[1,5,‡]
[1]*Department of Physics and Astronomy, Rutgers University, Piscataway, New Jersey 08854, USA*
[2]*Max Planck POSTECH/Korea Research Initiative, Pohang University of Science and Technology, Pohang 37673, Korea*
[3]*Laboratory of Pohang Emergent Materials, Pohang Accelerator Laboratory, Pohang 37673, Korea*
[4]*Rutgers Center for Emergent Materials, Rutgers University, Piscataway, New Jersey 08854, USA*
[5]*National Institute of Chemical Physics and Biophysics, 12618 Tallinn, Estonia*

(Received 30 August 2018; revised manuscript received 23 October 2018; published 9 November 2018)

We report *ab initio* density functional theory calculation and Raman scattering results to explore the electronic structure of $Ba_5CuIr_3O_{12}$ single crystals. This insulating iridate, consisting of face-sharing IrO_6 octahedra forming quasi-one-dimensional chains, cannot be described by the local $j_{\rm eff} = 1/2$ moment picture commonly adopted for discussing the electronic and magnetic properties of iridate compounds with IrO_6 octahedra. The shorter Ir-Ir distance in the face-sharing geometry, compared to corner- or edge-sharing structures, leads to strong covalency between neighboring Ir. Then, this strong covalency results in the formation of molecular orbitals (MOs) at each Ir trimer as the low-energy electronic degree of freedom. The theoretically predicted three-peak structure in the joint density of states, a distinct indication of deviation from the $j_{\rm eff} = 1/2$ picture, is verified by observing the three-peak structure in the electronic excitation spectrum by Raman scattering.

DOI: 10.1103/PhysRevB.98.201105

The competition between covalency and electron correlations is a core concept in the study of the Mott physics [1]. A canonical example is the contrast between the Mott insulating and metallic behaviors of 3*d* and 4*d* transition-metal oxides (TMOs), respectively. In these systems, the Mott phases in 3*d* TMOs are attributed to the smaller covalency of 3*d* orbitals, i.e., smaller overlap integrals and the resulting stronger Coulomb repulsion [2], while the enhanced covalency and weaker Coulomb repulsion in 4*d* TMOs lead to metallicity [3–5].

An interesting twist to the above simplistic picture happens in 5*d* TMOs, especially in iridate compounds with quasi-two-dimensional layered structures [6–9] where insulating behavior with local magnetic moments was found. The key to this puzzle was found to be the presence of the strong spin-orbit coupling (SOC) in the Ir 5*d* orbital. Namely, SOC introduces splitting of the broad 5*d* bands into narrow subbands and forms spin-orbital-entangled local moments identified with the effective total angular momentum $j_{\rm eff} = 1/2$ [10,11]. Since then, the $j_{\rm eff} = 1/2$ scenario has become a cornerstone in the study of correlated phases in 5*d* TMOs, and various theoretical suggestions of potential novel quantum phases such as high-T_c superconductivity [12,13] or quantum spin-liquid phases have been made based on this picture [14–16].

A critical necessary condition for the $j_{\rm eff} = 1/2$ picture is the presence of (pseudo)cubic IrO_6 octahedra, as shown in Fig. 1(a), where the Ir t_{2g} orbital ($l_{\rm eff} = 1$) splits into the $j_{\rm eff} = 1/2$ and 3/2 subspaces. Introducing noncubic crystal fields can mix the two $j_{\rm eff}$ subspaces and break the SU(2) symmetry of the $j_{\rm eff} = 1/2$ pseudospin. In various iridate compounds, however, such noncubic distortions of IrO_6 octahedra were found to be not strong enough to qualitatively change the $j_{\rm eff}$ picture [17–20], except in a small number of examples where the noncubic distortions are exceptionally huge [21]. Hence the belief for the validity of the $j_{\rm eff}$ scenario in general iridates has become strengthened, and it has been adopted even in situations where the applicability of the scenario is not rigorously justified [22].

In this Rapid Communication, we study a material in which the local $j_{\rm eff}$ moment picture breaks down, and the quenching of the SOC splitting occurs not because of the noncubic crystal fields, but because of the covalency between neighboring Ir *d* orbitals. The main message of this work is illustrated in Fig. 1, where the three representative local geometries consisting of IrO_6 octahedra—corner-, edge-, and face-sharing structures—are depicted. In terms of covalency, a critical difference between the three structures is the bond length between the nearest-neighboring Ir sites, which determines the strength of the Ir *d*-*d* direct overlap integral t_{dd} [23]. While t_{dd} tends to be smaller than the size of SOC ($\lambda_{\rm SO}$) for the corner- and edge-sharing geometries [Fig. 1(a)] [24], it can be stronger than $\lambda_{\rm SO}$ for the face-sharing structures because of the shorter Ir-Ir distance. In such cases, the neighboring Ir sites should form *molecular orbitals* (MOs) as depicted in Fig. 1(b). Therefore the $j_{\rm eff} = 1/2$ local moment picture in the face-sharing geometry breaks down and the effects of SOC and Coulomb interactions should be considered based on the MO description.

By combining Raman spectroscopy measurements and *ab initio* theoretical analyses, we study a mixed 3*d*-5*d* insulator $Ba_5CuIr_3O_{12}$ for which the $j_{\rm eff} = 1/2$ approach breaks

---

[*] mye@physics.rutgers.edu
[†] hk676@physics.rutgers.edu
[‡] girsh@physics.rutgers.edu

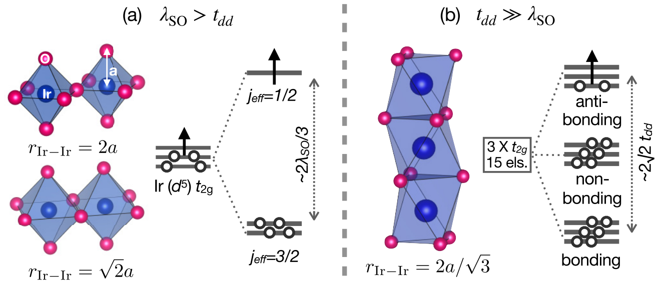

FIG. 1. Three representative local geometries consisting of IrO_6 octahedra and their schematic energy-level diagrams. (a) depicts corner- and edge-sharing geometries where the size of spin-orbit coupling (SOC) λ_{SO} is larger than the covalency between neighboring Ir $5d$ orbitals. (b) shows a face-sharing local geometry, where the Ir-O bond length is shorter compared to the other two cases so that the strength of d-d covalency t_{dd} can overcome SOC. Schematic energy-level diagrams for each case, the conventional atomic j_{eff} picture and a trimer molecular-orbital (MO) picture for (a) and (b), respectively, are represented.

down [25,26]. In this compound, sequences of trigonal prismatic and octahedral transition-metal sites run in chains parallel to the crystallographic z axis, with Ba atoms located between the chains (Fig. 2). *Ab initio* calculations and a tight-binding (TB) analysis yield a MO description of the electronic structure originating from the face-sharing geometry as depicted in Fig. 1(b), and predict a three-peak structure in the joint density of states (JDOS). Raman scattering, a technique successfully used to study electronic excitations in iridate compounds [27], verifies this prediction. We observe one strong and sharp excitation at 0.58 eV, and two weak features at 0.66 and 0.74 eV. It should be noted that such a three-peak structure is not observed in systems with well-defined $j_{eff} = 1/2$ local moments [27].

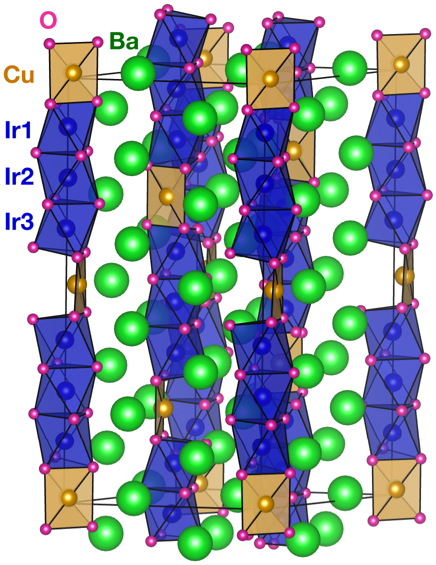

FIG. 2. $Ba_5CuIr_3O_{12}$ crystal structure employed for the *ab initio* calculations. Copper atoms are at the center of the prism face.

We identify the structural motif for $Ba_5CuIr_3O_{12}$ to be the three face-sharing IrO_6 octahedra forming an Ir trimer as shown in Figs. 1(b) and 2. If the intra-Ir-trimer hybridization dominates SOC, the three Ir t_{2g} orbitals at the trimer sites split into nine MOs [Fig. 3(a)]. Among those, the atomic a_{1g} singlet at each site gives rise to the strongest σ-type overlap between neighboring Ir sites, while the other e'_g doublets lead to weaker π- or δ-like overlaps. Such a scenario can be tested by constructing a simple TB model and comparing the results with those from density functional theory (DFT) calculations. For the TB model, as a first-order approximation, we assume a threefold symmetry along the z direction and ignore the Cu-Ir hybridization. After this simplification, just four free parameters are left for the Ir trimer model where the parameters are tuned to fit the DFT DOS afterwards [28,29]. Note that, because this is a test for the molecular orbital picture, SOC and the on-site Coulomb interactions are not considered at this stage.

Figure 3 presents the comparison between the TB model and the DFT results, where Figs. 3(a)–3(c) show the schematic TB energy diagram, TB DOS, and DFT DOS, respectively. Both the a_{1g}- and e'_g-derived MO states, depicted in blue and red in Fig. 3, show bonding ($\sigma/\pi/\delta$), nonbonding ($\bar{\sigma}/\bar{\pi}/\bar{\delta}$), and antibonding $\sigma^*/\pi^*/\delta^*$ characters [Fig. 3(a)]. Remarkably, the DOS from the simple four-parameter model agrees quite well with the DFT DOS; features of the DOS obtained from DFT calculations are consistent with those derived from

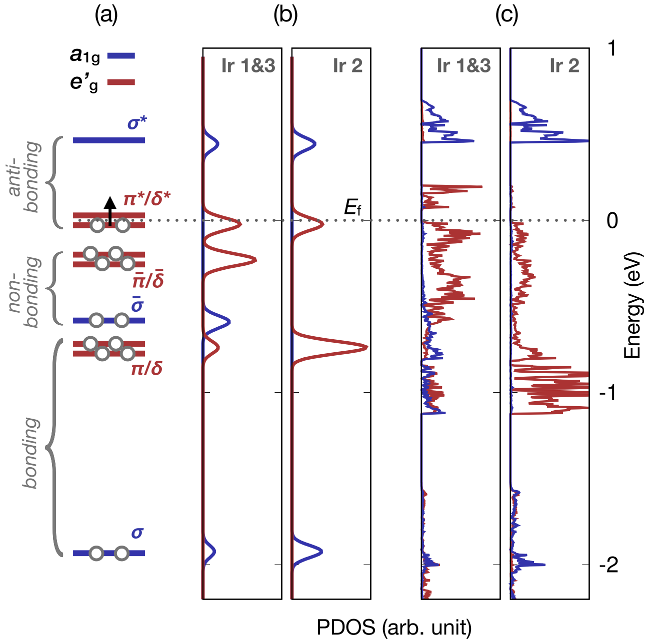

FIG. 3. (a) Energy-level diagram showing the splitting of the Ir t_{2g} states in an Ir trimer into MO states. Here, $\sigma/\pi/\delta$, $\bar{\sigma}/\bar{\pi}/\bar{\delta}$, and $\sigma^*/\pi^*/\delta^*$ denote bonding, nonbonding, and antibonding states, respectively. Electrons in fully filled states are represented by circles, while magnetically active electrons are represented by arrows. (b), (c) Projected DOS from the simple tight-bonding model for Ir trimers (b), and from *ab initio* calculations without SOC and magnetism (c). The color scheme for the orbital character is the same in (a)–(c).

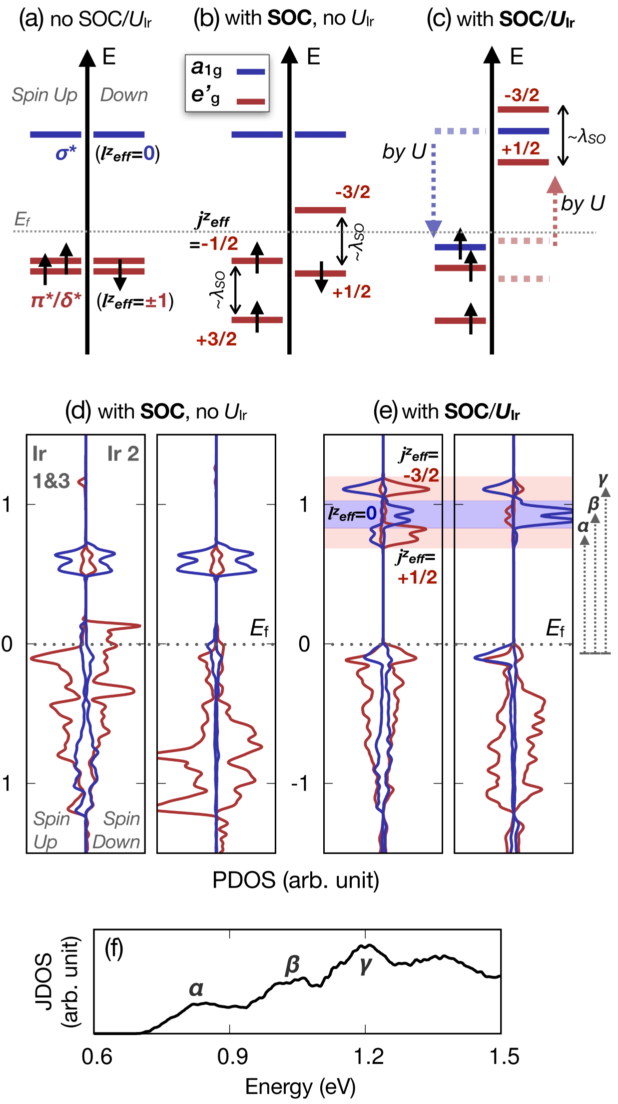

FIG. 4. (a)–(c) Schematic diagram showing the MO levels (a) with both SOC and U_{Ir} not included, (b) with SOC included but with no U_{Ir}, and (c) both SOC and U_{Ir} included (U_{Ir} denoting U at Ir sites). The l^z_{eff} and j^z_{eff} eigenvalues are given. (d), (e) Projected DOS from DFT+SOC+U calculations for the a_{1g} and e'_g states at Ir sites, where the U values employed are $(U_{\mathrm{Ir}}, U_{\mathrm{Cu}}) = (0, 6)$ eV and (2.8, 6) eV for (d) and (e), respectively (U_{Cu} denoting U at Cu sites). The blue and red curves in (a)–(e) depict the a_{1g} and e'_g characters, respectively. (f) The joint DOS (JDOS) with $(U_{\mathrm{Ir}}, U_{\mathrm{Cu}}) = (2.8, 6)$ eV, showing a three-peak structure (α, β, and γ).

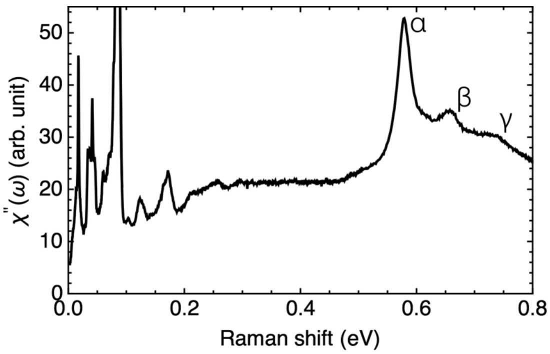

FIG. 5. Raman spectrum $\chi''(\omega)$ at 25 K. Sharp features below 0.1 eV are phonon modes; the two peaks at 0.13 and 0.17 eV result from second-order phonon scattering while the broad feature at 0.24 meV originates from third-order phonon scattering. The three high-energy electronic excitations at 0.58, 0.66, and 0.74 eV are labeled by α, β, and γ, respectively, corresponding to the labeling in Fig. 4(d).

the TB analysis, especially that the nonbonding $\bar{\sigma}/\bar{\pi}/\bar{\delta}$ MOs are located only at the two ends of the trimer [Figs. 3(b) and 3(c)]. The bonding-antibonding splitting between the σ and σ* MO is 2.5 eV, much larger than the strength of SOC (0.4 eV) [10]. Therefore the intra-Ir-trimer hybridization indeed dominates SOC.

Since the size of MO splitting is large, we only need to consider the effect of SOC near the Fermi level. Figure 4 illustrates how SOC and the Coulomb interaction induce a spin polarization within the σ*/π*/δ* MOs and in turn open a gap. First, because the π*/δ* MOs carry atomic orbital angular momenta $l^z_{\mathrm{eff}} = \pm 1$, the SOC functions as an orbital Zeeman field that splits the π*/δ* MOs [compare Figs. 4(a) and 4(b)]. Then, the Coulomb interaction induces a "high-spin-like" configuration by pushing the unoccupied σ* state with $l^z_{\mathrm{eff}} = 0$ below the Fermi level in the majority-spin channel and fully spin polarizing the π*/δ* and σ* states as shown in Fig. 4(c). Figures 4(d) and 4(e) show the projected DOS with $U_{\mathrm{Ir}} = 0$ and 2.8 eV, respectively (U_{Ir} denoting U at Ir sites), where the a_{1g}- and e'_g-projected DOS from the DFT+U [30] calculation with SOC included is plotted. Comparing Figs. 4(d) and 4(e) demonstrates the spin-polarizing effect of U_{Ir}.

As a result, a three-peak structure appears in the unoccupied sector as shown in Fig. 4(e). The three peaks, α, β, and γ in the JDOS from the DFT+U result [Fig. 4(f)], originate from the transitions from the highest occupied MO state with $j^z_{\mathrm{eff}} = 0$ to the unoccupied MO states with $j^z_{\mathrm{eff}} = +1/2$, 0, and −3/2, respectively. Note that the inclusion of U_{Ir} tends to recover the local atomic picture by mixing MO states, as shown in Fig. 4(e), where there is a small mixture among the $j^z_{\mathrm{eff}} = +1/2$, 0, and −3/2 MO states. This effect, however, does not qualitatively affect the above MO description. Note also that different values of U_{Ir} only change the gap size while not affecting the three-peak structure, as shown in the Supplemental Material [29].

To confirm the predicted three-peak structure in the electronic excitation spectrum, we perform Raman-scattering measurements in a quasibackscattering geometry from the (001) crystallographic surface of the $\mathrm{Ba_5CuIr_3O_{12}}$ single crystal grown by the flux method (see the Supplemental Material [29] for details of sample preparation and Raman scattering). We use the 476.2-nm line from a $\mathrm{Kr^+}$ ion laser for excitation. Incident light with ~10 mW power is focused to a 50 × 100 $\mu\mathrm{m}^2$ spot.

Figure 5 shows the Raman spectrum measured at 25 K. The sharp features at 17, 41, and 84 meV are phonon modes (see the Supplemental Material [29] for the low-energy Raman spectrum). The two peaks at 130 and 170 meV result from second-order phonon scattering (41 + 84 and 84 + 84 meV, respectively). The broad feature centered at 240 meV, weaker and broader than the second-order phonon scattering peaks, is attributed to third-order phonon scattering (84 + 84 + 84 meV).

Importantly, three high-energy electronic excitations at 0.58, 0.66, and 0.74 eV are resolved. The high-energy Raman spectrum exhibits the general trends of the JDOS from DFT+U. The high-energy gap in the Raman spectrum is about 0.55 eV, while it is 0.70 eV in the JDOS. The three peaks in the Raman spectrum are evenly spaced, with a separation of 0.08 eV; those in the JDOS are also evenly spaced but with a 0.2-eV separation. One possible reason for the smaller splitting in the experimental spectrum compared to the DFT+U JDOS peak splitting can be a stronger mixing between the $l^z_{\rm eff} = \pm 1$ and 0 antibonding MO states near the Fermi level in the real system. This mixing reduces the expectation value of SOC energy and in turn decreases the separation. We also mention that, while in the JDOS all the three peaks have a similar spectral weight, in the Raman spectrum the 0.58-eV peak is much stronger than the other two. This could be attributed to the matrix element effect.

The three-peak structure in the DFT+U JDOS and in the Raman measurement is a distinct feature indicating deviation from the $j_{\rm eff} = 1/2$ picture. A simple $j_{\rm eff} = 1/2$ picture predicts up to two high-energy transition peaks, because noncubic crystal fields just induce splitting of the fully occupied $j_{\rm eff} = 3/2$ quartet [10,18]. On the contrary, our three-peak structure in $Ba_5CuIr_3O_{12}$ comes from the strong Ir-Ir hybridization in the face-sharing IrO_6 octahedral geometry and the resulting formation of MOs. We note that in other compounds with similar face-sharing geometries with alternating 3d and 5d transition-metal ions such as Sr_3NiIrO_6 [31] or Sr_3CuIrO_6 [20], two-peak structures are observed in their $j_{\rm eff}$-excitation spectra [18]. This implies that, although the size of noncubic distortions is large in these compounds, still the local $j_{\rm eff} = 1/2$ moment picture remains effective because of the reduced covalency between the 3d and 5d orbitals as suggested in a recent *ab initio* study for Sr_3NiIrO_6 [32]. We also comment that there is another theoretical study on $BaIrO_3$ [22], consisting of the same face-sharing Ir_3O_{12} octahedral trimers as $Ba_5CuIr_3O_{12}$. A similar three-peak structure in the upper Hubbard band (UHB) was reported therein, but it was speculated that the UHB states still retain the $j_{\rm eff} = 1/2$ character, which seems to require a more rigorous justification.

As for possible magnetism in this compound, from the projected DOS plotted in Figs. 4(b) and 4(c), we identify three magnetically active states: a σ^* state with mostly a_{1g} ($l^z_{\rm eff} = 0$) character mainly located at the Ir 2 site, and two π^*/δ^* states with the e'_g character ($l^z_{\rm eff} = \pm 1$) at Ir 1 and 3 sites. The strong SOC within the Ir d orbital then behaves as a single-ion anisotropy to the electron spins filling the $l^z_{\rm eff} = \pm 1$ MO states, locking the spins parallel to the z direction. Spin in the $l^z_{\rm eff} = 0$ MO state, on the other hand, has little single-ion anisotropy due to the vanishing orbital angular momentum. The spin moments at Cu sites are also isotropic, so this compound should have three different kinds of spin moments: isotropic Cu spins, isotropic Ir spins at Ir 2 sites, and anisotropic Ir spins at Ir 1 and 3 sites locked along the z direction. Because all the Ir spins are occupying the MO states, rather than behaving as the $j_{\rm eff} = 1/2$ local moments, they may show distinct low-energy magnetic properties compared to previously known magnetic iridate compounds. For future studies, interesting questions about the outcome of MO formation can be posed, for example, on the form of exchange interactions and the spectrum of low-energy magnetic excitations.

Our study on the face-sharing iridate $Ba_5CuIr_3O_{12}$ demonstrates the breakdown of the SOC-based $j_{\rm eff} = 1/2$ physics, and reveals the MO nature of the electronic structure originating from the strong intermetallic d-d direct overlap. A similar scenario, leading to the formation of benzene-ring-shaped quasimolecular orbitals (QMOs) driven by a π-like d-p overlap, was suggested for Na_2IrO_3 [33]. In Na_2IrO_3, the d-p overlap preserves the threefold symmetry of the Ir t_{2g} orbitals, hence the inclusion of SOC and U induces a crossover from the delocalized QMO to the local $j_{\rm eff} = 1/2$ moment picture [34]. In $Ba_5CuIr_3O_{12}$, on the contrary, the direct overlap t_σ is not only huge but also explicitly breaks the degeneracy of the Ir t_{2g} orbitals, resulting in a completely different MO description. Overall, this work suggest a peculiar relation between the crystal structure and the nature of electronic degree of freedom in 5d iridates and other transition-metal compounds, which can be useful in the search for novel correlated materials.

We thank H.-H. Kung for comments on an early version of the manuscript. The crystal growth (C.-J.W.) was supported by the National Research Foundation of Korea, Ministry of Science and ICT (No. 2016K1A4A4A01922028). The *ab initio* DFT study (H.-S.K., D.V., K.H.) and the crystal characterization (J.-W.K., S.-W.C.) were supported by NSF DMREF DMR-1629059. The spectroscopic work (M.Y., G.B.) was supported by NSF Grant No. DMR-1709161. M.Y. and H.-S.K. contributed equally to this work.

---

[1] M. Imada, A. Fujimori, and Y. Tokura, Rev. Mod. Phys. **70**, 1039 (1998).

[2] D. I. Khomskii, *Transition Metal Compounds* (Cambridge University Press, Cambridge, U.K., 2014).

[3] P. A. Cox, Metallic oxides, in *Transition Metal Oxides: An Introduction to Their Electronic Structure and Properties* (Oxford University Press, Oxford, U.K., 1992), pp. 204–276.

[4] A. Damascelli, D. H. Lu, K. M. Shen, N. P. Armitage, F. Ronning, D. L. Feng, C. Kim, Z.-X. Shen, T. Kimura, Y. Tokura, Z. Q. Mao, and Y. Maeno, Phys. Rev. Lett. **85**, 5194 (2000).

[5] F. Baumberger, N. J. C. Ingle, W. Meevasana, K. M. Shen, D. H. Lu, R. S. Perry, A. P. Mackenzie, Z. Hussain, D. J. Singh, and Z.-X. Shen, Phys. Rev. Lett. **96**, 246402 (2006).

[6] M. K. Crawford, M. A. Subramanian, R. L. Harlow, J. A. Fernandez-Baca, Z. R. Wang, and D. C. Johnston, Phys. Rev. B **49**, 9198 (1994).

[7] H. Okabe, M. Isobe, E. Takayama-Muromachi, A. Koda, S. Takeshita, M. Hiraishi, M. Miyazaki, R. Kadono, Y. Miyake, and J. Akimitsu, Phys. Rev. B **83**, 155118 (2011).

[8] Y. Singh and P. Gegenwart, Phys. Rev. B **82**, 064412 (2010).

[9] K. Ohgushi, J.-i. Yamaura, H. Ohsumi, K. Sugimoto, S. Takeshita, A. Tokuda, H. Takagi, M. Takata, and T.-h. Arima, Phys. Rev. Lett. **110**, 217212 (2013).

[10] B. J. Kim, H. Jin, S. J. Moon, J.-Y. Kim, B.-G. Park, C. S. Leem, J. Yu, T. W. Noh, C. Kim, S.-J. Oh, J.-H. Park, V. Durairaj, G. Cao, and E. Rotenberg, Phys. Rev. Lett. **101**, 076402 (2008).

[11] B. J. Kim, H. Ohsumi, T. Komesu, S. Sakai, T. Morita, H. Takagi, and T. Arima, Science **323**, 1329 (2009).

[12] Y. K. Kim, O. Krupin, J. D. Denlinger, A. Bostwick, E. Rotenberg, Q. Zhao, J. F. Mitchell, J. W. Allen, and B. J. Kim, Science **345**, 187 (2014).

[13] Y. K. Kim, N. H. Sung, J. D. Denlinger, and B. J. Kim, Nat. Phys. **12**, 37 (2015).

[14] G. Jackeli and G. Khaliullin, Phys. Rev. Lett. **102**, 017205 (2009).

[15] W. Witczak-Krempa, G. Chen, Y. B. Kim, and L. Balents, Annu. Rev. Condens. Matter Phys. **5**, 57 (2014).

[16] J. G. Rau, E. K.-H. Lee, and H.-Y. Kee, Annu. Rev. Condens. Matter Phys. **7**, 195 (2016).

[17] H. Zhang, K. Haule, and D. Vanderbilt, Phys. Rev. Lett. **111**, 246402 (2013).

[18] H. Gretarsson, J. P. Clancy, X. Liu, J. P. Hill, E. Bozin, Y. Singh, S. Manni, P. Gegenwart, J. Kim, A. H. Said, D. Casa, T. Gog, M. H. Upton, H.-S. Kim, J. Yu, V. M. Katukuri, L. Hozoi, J. van den Brink, and Y.-J. Kim, Phys. Rev. Lett. **110**, 076402 (2013).

[19] L. Hozoi, H. Gretarsson, J. P. Clancy, B.-G. Jeon, B. Lee, K. H. Kim, V. Yushankhai, P. Fulde, D. Casa, T. Gog, J. Kim, A. H. Said, M. H. Upton, Y.-J. Kim, and J. van den Brink, Phys. Rev. B **89**, 115111 (2014).

[20] X. Liu, V. M. Katukuri, L. Hozoi, W.-G. Yin, M. P. M. Dean, M. H. Upton, J. Kim, D. Casa, A. Said, T. Gog, T. F. Qi, G. Cao, A. M. Tsvelik, J. van den Brink, and J. P. Hill, Phys. Rev. Lett. **109**, 157401 (2012).

[21] S.-W. Kim, C. Liu, H.-J. Kim, J.-H. Lee, Y. Yao, K.-M. Ho, and J.-H. Cho, Phys. Rev. Lett. **115**, 096401 (2015).

[22] W. Ju, G.-Q. Liu, and Z. Yang, Phys. Rev. B **87**, 075112 (2013).

[23] S. V. Streltsov and D. I. Khomskii, Proc. Natl. Acad. Sci. USA **113**, 10491 (2016).

[24] Several recent reports of pressure-induced Ir dimerizations in layered- and hyperhoneycomb iridates [35,36] imply that, in edge-sharing geometries, t_{dd} is almost comparable to $\lambda_{\rm SO}$, so that a relatively small pressure of <5 GPa is enough to enhance t_{dd} to break the $j_{\rm eff} = 1/2$ states in these compounds.

[25] G. R. Blake, J. Sloan, J. F. Vente, and P. D. Battle, Chem. Mater. **10**, 3536 (1998).

[26] G. R. Blake, P. D. Battle, J. Sloan, J. F. Vente, J. Darriet, and F. Weill, Chem. Mater. **11**, 1551 (1999).

[27] J.-A. Yang, Y.-P. Huang, M. Hermele, T. Qi, G. Cao, and D. Reznik, Phys. Rev. B **91**, 195140 (2015).

[28] For the DFT calculations we employed the Vienna *ab initio* simulation package (VASP) [37,38] with PBEsol [39] and DFT+U [30] functionals.

[29] See Supplemental Material at http://link.aps.org/supplemental/10.1103/PhysRevB.98.201105 for the details of the TB model, DFT calculations, and Raman measurements.

[30] S. L. Dudarev, G. A. Botton, S. Y. Savrasov, C. J. Humphreys, and A. P. Sutton, Phys. Rev. B **57**, 1505 (1998).

[31] E. Lefrançois, A.-M. Pradipto, M. Moretti Sala, L. C. Chapon, V. Simonet, S. Picozzi, P. Lejay, S. Petit, and R. Ballou, Phys. Rev. B **93**, 224401 (2016).

[32] T. Birol, K. Haule, and D. Vanderbilt, Phys. Rev. B **98**, 134432 (2018).

[33] I. I. Mazin, H. O. Jeschke, K. Foyevtsova, R. Valentí, and D. I. Khomskii, Phys. Rev. Lett. **109**, 197201 (2012).

[34] K. Foyevtsova, H. O. Jeschke, I. I. Mazin, D. I. Khomskii, and R. Valentí, Phys. Rev. B **88**, 035107 (2013).

[35] L. S. I. Veiga, M. Etter, K. Glazyrin, F. Sun, C. A. Escanhoela, G. Fabbris, J. R. L. Mardegan, P. S. Malavi, Y. Deng, P. P. Stavropoulos, H.-Y. Kee, W. G. Yang, M. van Veenendaal, J. S. Schilling, T. Takayama, H. Takagi, and D. Haskel, Phys. Rev. B **96**, 140402 (2017).

[36] V. Hermann, M. Altmeyer, J. Ebad-Allah, F. Freund, A. Jesche, A. A. Tsirlin, M. Hanfland, P. Gegenwart, I. I. Mazin, D. I. Khomskii, R. Valentí, and C. A. Kuntscher, Phys. Rev. B **97**, 020104 (2018).

[37] G. Kresse and J. Furthmüller, Phys. Rev. B **54**, 11169 (1996).

[38] G. Kresse and D. Joubert, Phys. Rev. B **59**, 1758 (1999).

[39] J. P. Perdew, A. Ruzsinszky, G. I. Csonka, O. A. Vydrov, G. E. Scuseria, L. A. Constantin, X. Zhou, and K. Burke, Phys. Rev. Lett. **100**, 136406 (2008).